ARTICLES SCIENCE CHINA Materials

mater.scichina.com link.springer.com

Published online 5 March 2020 | https://doi.org/10.1007/s40843-020-1271-x
Sci China Mater 2020, 63(6): 982–992

SPECIAL TOPIC: Single-atom Catalysts

Single-atom Pd dispersed on nanoscale anatase TiO_2 for the selective hydrogenation of phenylacetylene

Fu Yang[1,2], Shipeng Ding[1*], Hongbing Song[3] and Ning Yan[1*]

ABSTRACT **Combining the advantages of both heterogeneous and homogeneous catalysts, single-atom catalysts (SACs) with unique electronic properties have shown excellent catalytic properties. Herein, we report single-atom Pd dispersed on nanoscale TiO_2 prepared by self-assembly method as efficient and selective catalysts for the hydrogenation of phenylacetylene to styrene. The catalysts were characterized by N_2 adsorption/desorption, X-ray diffraction (XRD), transmission electron microscopy (TEM), X-ray photoelectron spectroscopy (XPS), diffuse reflectance infrared Fourier transform spectroscopy (DRIFTS) and X-ray absorption spectroscopy (XAS). 0.2Pd-TiO_2(150°C) possessing dominant single-atom Pd species, exhibited a turnover frequency (TOF) of over 8000 h^{-1} with 91% selectivity towards styrene at room temperature. Further increasing Pd loading from 0.2% to 0.5% and 1.5% resulted in the decrease of activity probably due to the formation of Pd nanoparticles. Besides, the 0.2Pd-TiO_2 prepared by self-assembly strategy showed better catalytic performance than commercial 10%Pd/C and 0.2Pd-TiO_2 synthesized by using impregnation method.**

Keywords: single-atom catalyst, palladium, nanoscale TiO_2, semihydrogenation, self-assembly method

INTRODUCTION

Single-atom catalysts (SACs) with maximum utilization efficiency of metal atoms have emerged as promising catalytic systems, attracting progressive research attention [1–17]. Besides, the SACs offer an ideal model to further understand the heterogeneous catalytic process at the molecular level, thereby bridging the gap between heterogeneous and homogeneous catalysis [18]. From application perspective, SACs are also desirable due to the low abundance, high price and rapid consumption of noble metals. However, how to avoid or diminish the deactivation of the SACs remains an issue due to the high free energy and mobility of the isolated metal atoms. The stability of catalytic metal species is strongly dependent on the support [19,20], and the supports to anchor single-atom species are deliberately selected in most cases. So far, a number of single-atom catalysts have been synthesized through confining the metal species within the microporous structure of the support, or enhancing the metal-support interactions [21–30]. For example, defects or enriched oxygen compositions on the surface of reducible oxides (e.g., TiO_2 and CeO_2) are capable of stabilizing atomically dispersed metal species [31–35]. Two-dimensional or porous materials are favorable for the atomic dispersion of metal species due to their large surface areas [36–43]. Considering that the inter-particle migration of metal atom species usually needs to overcome much higher energy barrier than that on the surface of the same particle, decreasing the size of the support may be a viable way to prohibit the aggregation of single metal atoms. Besides, it is interesting to explore the catalytic performance of single-atom metal dispersed on nanosized support, taking the advantages of the unique properties of both the nanoscale support and single metal atoms.

Semihydrogenation of alkyne such as phenylacetylene is a process of great importance in industry as the trace amount of alkyne usually causes the deactivation of the alkene polymerization catalysts. It has been reported that SACs showed higher alkyne and diene hydrogenation selectivity towards alkene due to the absence of adjacent metal atoms in comparison with nanoparticle counterparts [9]. Single-atom Pd_1/graphene prepared by atomic layer deposition technique showed 100% butenes se-

[1] Department of Chemical and Biomolecular Engineering, National University of Singapore, 4 Engineering Drive 4, 117585, Singapore
[2] School of Environmental and Chemical Engineering, Jiangsu University of Science and Technology, Zhenjiang 212003, China
[3] College of Chemical Engineering, Qingdao University Science & Technology, Qingdao 266042, China
* Corresponding authors (emails: ning.yan@nus.edu.sg (Yan N); shipengding@u.nus.edu (Ding S))

lectivity with 95% conversion at 50°C in 1,3-butadiene hydrogenation [44]. Cu-alloyed Pd SAC exhibited 100% acetylene conversion and 85% ethylene selectivity [45]. The electron transfer from Cu to Pd promoted the dissociation of H_2 and the desorption of ethylene. It was also reported that single-atom Pd anchored on Cu surface facilitated the activation of H_2 at single-atom Pd sites and the desorption of H atoms from Cu metal surface during the hydrogenation of acetylene [46]. Both experimental data and theoretical calculation showed that SAC Pt gave a lower H_2 adsorption energy compared with Pt clusters or nanoparticles [19]. The alkyne semihydrogenation activity of single-atom Au was dependent on the substrates: structure insensitive for alkynols with γ-OH and unfunctionalized alkynes, while sensitive for alkynols with α-OH [47]. More recently, Ma and co-workers [48] reported that non-noble metal SACs Cu supported on nanodiamond-graphene exhibited 95% acetylene conversion and 98% ethylene selectivity.

Herein, we disperse single Pd atoms on nanoscale TiO_2 *via* a self-assembly method, as an extension of our previous work on the Pt_1/Al_2O_3 system [42]. The nanoscale TiO_2 carrier affords high surface area, thanks to the addition of the ploy-block copolymer P123 during catalyst synthesis. The prepared single-atom 0.2Pd-TiO_2(150°C) catalyst showed better activity and selectivity in phenylacetylene selective hydrogenation in comparison to 0.2Pd-TiO_2 synthesized by the impregnation method. The excellent catalytic performance of single-atom 0.2Pd-TiO_2 was attributed to the unique electronic structure of single-atom Pd and nanoscale TiO_2.

EXPERIMENTAL SECTION

Chemicals

Triblock copolymer Pluronic®123 (PEO-PPO-PEO, molecular weight ~5800), titanium (IV) isopropoxide (TIP, 99%), phenylacetylene (98%) and commercial titanium oxide P25 (size ~25 nm) were purchased from Sigma-Aldrich. Palladium chloride ($PdCl_2$, Pd>67%) was purchased from Sinopharm Co., Ltd. Ethanol (absolute), and methanol (AR) were from Fisher Scientific. Hydrochloric acid (32%) and sulfur acid (96%), ethyl acetate (AR) were supplied by Merk Pte. Ltd. Lindlar catalyst was purchased from Aldrich Reagent Int., with Pd (5 wt%) poisoned by a lead complex. All chemicals were used as received.

Synthesis of atomic-scale Pd supported size-tailored nanoanatase TiO_2

In a typical procedure, 1.0 g of Pluronic P123 was completely dissolved in 30 g of ethanol at room temperature. Concentrated H_2SO_4 (96% 0.55 g) and concentrated HCl (32%, 1.5 g) were sequentially added to the above mixed ethanol solution, followed by 2 h stirring at room temperature. TIP (3.6 g) was added to the mixed solution and vigorously stirred for another 6 h. Then the $PdCl_2$ solution (0.1 mol L^{-1}) with controlled volume was added with additional 24 h stirring at room temperature. The resulting solution (gel) was transferred into a Petri dish, and evaporated in the fume hood at room temperature for three days. The obtained gels were dried in a 60°C oven for 12 h, calcined at 350°C for 1 h and finally calcined at 450°C for 5 h to produce the as-synthesized Pd supported TiO_2. The resulted catalysts were designated as 0.2Pd-TiO_2(O), 0.5Pd-TiO_2(O), 1.5Pd-TiO_2(O) accordingly. The catalysts were reduced using the 5% H_2/N_2 mixed gas at 150°C for 1 h. The obtained final catalysts were designated as 0.2Pd-TiO_2(150°C), 0.5Pd-TiO_2(150°C), and 1.5Pd-TiO_2(150°C) accordingly. The blank comparative TiO_2 was obtained using the same synthetic procedure without adding H_2PdCl_4.

The post-treated sample was synthesized by the wet-impregnation method using the pure nanoanatase fabricated above to impregnate the same amount of H_2PdCl_4 solution and followed by the collection and calcination. The resulting sample was labeled as 0.2Pd-TiO_2(post-O)/(post-R) (R represents reduced temperature). The comparative catalyst samples without adding P123 were synthesized according to the aforementioned procedure, and these resultant samples were labeled as 0.2Pd-TiO_2(w-R), 0.5Pd-TiO_2(w-R), and 1.5Pd-TiO_2(w-R).

Characterizations

The structure properties of catalysts were measured by N_2 adsorption/desorption at 77 K (NOVA3200e, Quantachrome). The sample was first degassed at 120°C for 12 h. The surface area was analyzed by Brunauer-Emmet-Teller (BET) method, and the pore size distribution was determined using Barrett-Joyner-Halenda (BJH) method. Transmission electron microscopy (TEM) was carried out at 200 kV on a JEM 2100F microscope (JEOL, Japan). The sample was further examined with the energy-dispersive X-ray (EDX) mapping technique by the equipped EDX accessory. X-ray diffraction (XRD) measurement was done at a scan rate of 2°/min (Bruker D8 Advance X-Ray Diffractometer), applying a voltage of 40 kV and a current of 30 mA.

X-ray photoelectron spectra (XPS) of Pd-TiO_2 samples were obtained on a VG Escalab MKII spectrometer equipped with a mono Al Kα X-ray source (hv =

1486.71 eV, 5 mA, 15 kV). The spectra were internally calibrated by setting the binding energy of C 1s as 284.6 eV. The percentage of Pd in Pd-TiO_2 catalysts was measured by inductively coupled plasma optical emission spectrometry (ICP-OES). The samples were decomposed with concentrated aqua regia at 80°C for 4 h before ICP-OES measurement.

Fourier transform infrared spectroscopy of 0.2Pd-TiO_2 (150°C) was collected on Bruker VECTOR22 resolution. Diffuse reflectance infrared Fourier transform spectroscopy (DRIFTS) was performed as the procedure reported before [42]. The spectra were collected at room temperature with a resolution of 4 cm^{-1} from 2300 to 1800 cm^{-1}. The X-ray absorption spectra (XAS) of Pd-TiO_2 samples were measured at the BL01B1 beamline in the Spring-8, Japan. The spectra were analyzed using Athena and Artemis, and the theoretical scattering path was generated with FEFF 6.0L.

Catalytic assessment

The selective hydrogenation of phenylacetylene using the obtained catalysts was performed in a 15-mL autoclave equipped with a magnetic stirrer. In a typical procedure, reaction substrate (224 μL, 2 mmol), a desirable amount of catalyst, and a certain amount of methanol solvent (3 mL) were added into the above autoclave. The reaction was purged with pure H_2 several times and before a final charging of H_2 at room temperature to 10 bar. The reaction duration was 30 min. The resulting mixture in the autoclave was filtered with a poly(tetrafluoroethylene) (PTFE) syringe filter and analyzed by gas chromatograph (GC) Agilent 7890C GC with an HP-5/BP-5 column and a flame ionization detector (FID).

RESULTS AND DISCUSSION

Synthesis of Pd-TiO_2 catalysts

The carrier plays a crucial role in the stabilization and electronic modulation of single metal atoms. Anatase TiO_2 crystals have specific physicochemical characteristics, while nanosized anatase TiO_2 affords improved properties in the context of supporting atomically dispersed metal species. For example, it provides a larger surface to accommodate more single metal atoms and eliminates the external diffusing effect of reactant molecules during catalysis. More importantly, a dramatic barrier for the migration of metal atoms is achieved by generating nanoscale carriers. In this work, the single-atom Pd supported on nanoanatase TiO_2 was prepared by the sol-gel solvent evaporation self-assembly method. As shown in Scheme 1, TIP was used as the Ti precursor, and P123 was acted as the dispersant to obtain the nanosized anatase TiO_2. The air-calcination process induced the removal of organic species P123 (Fig. S1a) and the formation of anatase crystals. The final Pd-TiO_2 was obtained by H_2 reduction to remove chlorine and surface oxygen moiety partially. The H_2 temperature programmed reduction (H_2-TPR) for Pd-TiO_2(O) was also performed and no reduction peak assigned to Pd species was identified due to the low Pd loading (Fig. S1b). The peak at around 530°C was ascribed to the reduction of TiO_2. Normally, the reduction of TiO_2 was difficult below 750°C. The presence of Pd significantly decreased the reduction temperature of TiO_2 as a result of H_2 spillover for the 0.2Pd-TiO_2(O) sample. As shown in Fig. S2a, a broad Cl peak at around 199 eV was observed on 0.2Pd-TiO_2(O), but no Cl peak was identified after the sample reduction at 150°C, confirming the removal of Cl. The Pd XPS of Pd-TiO_2 before and after H_2 reduction were shown in Fig. S2b and c, respectively. The binding energy decreased significantly after H_2 reduction, hinting at partial removal of the surface oxygen atoms.

Characterizations of Pd-TiO_2 Catalyst

Nitrogen adsorption/desorption measurement was utilized to probe the structural characteristics of the prepared catalysts. As observed in Fig. 1, a type-IV isotherm and big hysteresis loop at high P/P_0 emerged as the typical

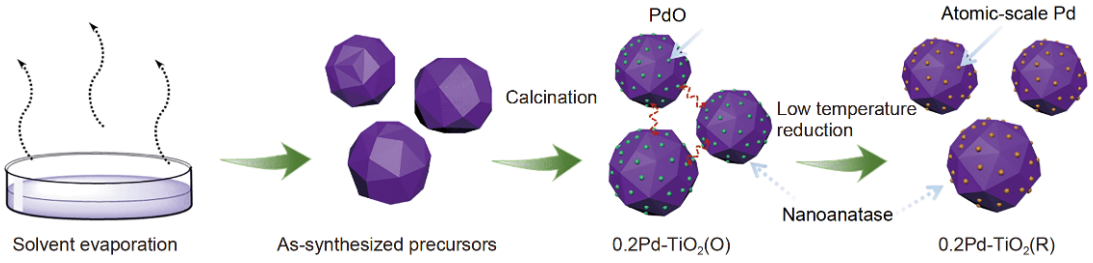

Scheme 1 Schematic synthetic illustration for constructing single-atom Pd supported on nanoscale TiO_2.

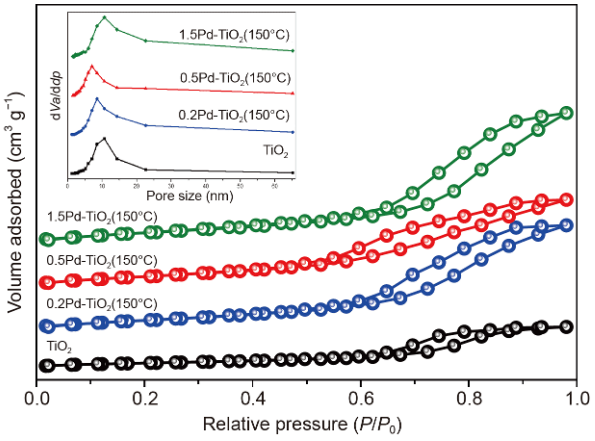

Figure 1 N_2 adsorption/desorption isotherms and corresponding pore size distribution (insert) of pure TiO_2, 0.2Pd-TiO_2(150°C), 0.5Pd-TiO_2(150°C), and 1.5Pd-TiO_2(150°C).

characteristic of packing mesoporous materials [49,50]. These packing mesopores might be derived from the voids of interparticle, which were associated with the promotion of long-chain block polymer P123. The corresponding pore size distribution of the packing voids calculated from the BJH method (insert) verified a pore range of 7–12 nm. The surface area calculated by BET method ranged from 94 to 135 $m^2 g^{-1}$. Interestingly, the surface area of the catalysts showed an increasing trend with the enhanced loading of Pd in the samples. Detail textural parameters are listed in Table 1. The synthesized Pd-TiO_2(O) samples exhibited similar absorption-desorption isotherms compared with samples before H_2 reduction (Fig. S3), suggesting the preservation of catalyst porosity during H_2 reduction.

The powder wide-angle X-ray diffraction (XRD) patterns of the catalysts before and after H_2 reduction (150°C) were presented to further probe the influence of H_2 reduction on catalyst structure. As shown in Fig. 2, the XRD patterns of various samples confirm that all obtained catalysts only afford highly crystalline anatase TiO_2 phase (JCPDS # No. 21-1272; Space group *I*41/*amd*) [51]. The diffraction peaks centered at 2θ = 25.3°, 37.9°, 48.0°, 53.9°, 55.1°, 62.7°, 68.9°, 70.2°, 75.2°, and 82.8° are identified and indexed to (101), (004), (200), (105), (211), (204), (116), (220), (215) and (224) crystal facets of anatase phase TiO_2, respectively. The H_2 reduction at 150°C did not induce obvious variation of the nanoscale anatase TiO_2 structure. Note that no diffraction peaks ascribed to Pd species were observed on 1.5Pd-TiO_2 after H_2 reduction treatment, indicating the existence of the strong interaction between Pd and nanoscale TiO_2 support. The post-synthesized catalysts including 0.2Pd-TiO_2(post-O) and 0.2Pd-TiO_2(post-R) were further checked by wide-angle XRD (Fig. S4); however, no detectable differences were observed for the Pd species probably because of the low Pd loading.

To ascertain the microscale structure of nanoanatase TiO_2 and the dispersion state of noble metal Pd, TEM was employed, and the representative TEM images of 0.2Pd-TiO_2(150°C), 0.5Pd-TiO_2(150°C), and 1.5Pd-TiO_2(150°C) were displayed in Fig. 3. The TiO_2 nanoparticles afforded an average size of around 12 nm. The unreduced catalysts containing different Pd loadings were also examined by TEM (Fig. S5). No obvious changes in morphology and structure of catalysts before and after H_2 reduction were detected, further confirming that H_2 reduction at 150°C hardly affected the microscale structure of Pd-TiO_2 catalysts. It should be noted that Pd species were not detected in the presented TEM images, indicating the good dispersion of Pd in those samples. The high-resolution TEM images (insert in Fig. 3a) showed well-defined lattice plane of anatase TiO_2, in good agreement with XRD data shown above. To identify the distribution of species, the elemental mapping technique was utilized to extract the element Ti, O, and Pd from the selected area of 0.2Pd-TiO_2(150°C). The results revealed that Ti and O afforded serried distribution on the samples, while Pd showed sparsely-distributed state due to its low loading.

To confirm the function of the constructed significant physical migration gap for the supported Pd species between the separated interparticles, we designed a control

Table 1 Textural properties of several involved comparative samples

Sample	Loading of Pd (wt%)[a]	S_{BET} ($m^2 g^{-1}$)	Pore volume ($cm^3 g^{-1}$)	Pore size D_{BJH} (nm)
Pure TiO_2	0	94.3	0.238	8.5
0.2Pd-TiO_2(150°C)	0.203	121.4	0.308	8.6
0.5Pd-TiO_2(150°C)	0.497	119.5	0.260	7.1
1.5Pd-TiO_2(150°C)	1.505	135.8	0.377	10.7

a) Metal loadings were calculated from the ICP results.

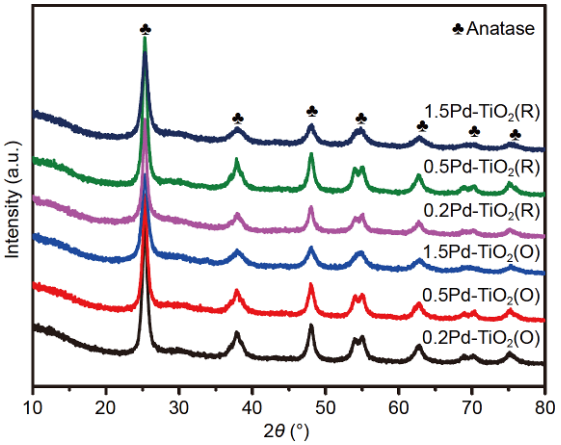

Figure 2 Wide-angle XRD patterns of Pd-TiO_2 serial catalysts before and after H_2 reduction at 150°C for 1 h.

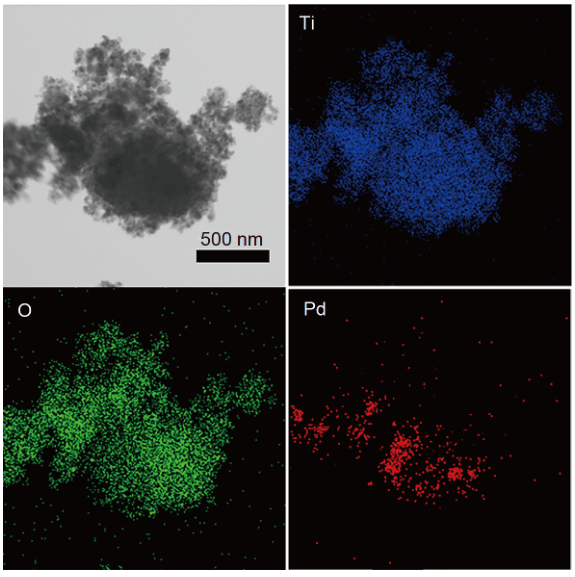

Figure 4 TEM images and elemental mapping results derived from mechanical mixed P25 and 3Pd-TiO_2(O) after calcination under 400°C for 5 h.

experiment by mechanically mixing 3Pd-TiO_2(O) and P25(commercial), followed by the calcination procedure at 400°C for 5 h. The resulting mixed sample was checked in detail by TEM and elemental mapping techniques. As shown in Fig. 4, the TEM images demonstrate that the resulting sample consists of the packing TiO_2 nanoparticles. Meantime, notably, the uniform distribution of Ti and O on the selective area can be clearly identified in the elemental mapping results. However, as expected, the partially serried appearance of Pd on the selective area of the sample was discriminatively observed, which might be attributed to the supported Pd on 3Pd-TiO_2(O). The serried dispersion of Pd at the partial position of sample demonstrated the limited migration of Pd atoms between TiO_2 particles under high-temperature driving force (400°C). The results supported the proposed strategy by using separated nano-carriers. On the other hand, samples with the controlled Pd loadings synthesized in the absence of P123 were utilized to ascertain the function of P123. Representative TEM images of 0.2Pd-TiO_2(w-R), 0.5Pd-TiO_2(w-R), 1.5Pd-TiO_2(w-R), and 0.2Pd-TiO_2(post-150°C) are displayed in Fig. 5. The obvious aggregation and crosslinking of the resulting TiO_2 were observed in samples without P123, proving the promising dispersion-promoting functionality and hole-forming effect of long-

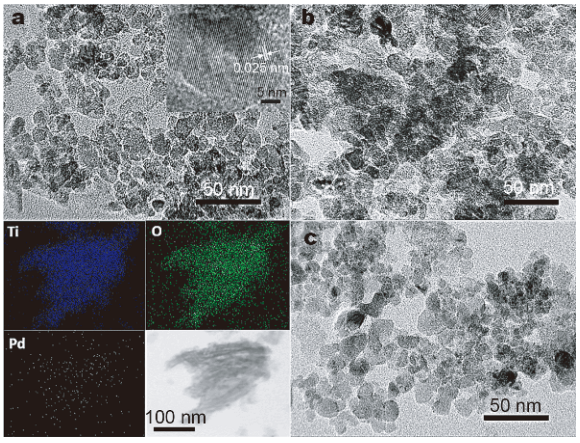

Figure 3 Representative TEM images of (a) 0.2Pd-TiO_2(150°C), (b) 0.5 Pd-TiO_2(150°C), (c) 1.5 Pd-TiO_2(150°C) and (d) the elemental mapping results of 0.2Pd-TiO_2(150°C).

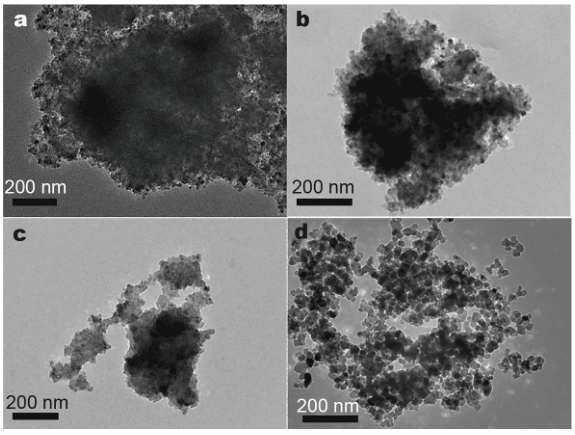

Figure 5 Representative TEM images of samples synthesized without P123 and post-impregnated P25 (a) 0.2Pd-TiO_2(w-R), (b) 0.5Pd-TiO_2 (w-R), (c) 1.5Pd-TiO_2(w-R), and (d) 0.2Pd-TiO_2(post-150°C).

chain block polymer P123 during the synthesis procedure.

To accurately identify the chemical state of surface elements on the catalysts, XPS was employed to ascertain 0.2Pd-TiO_2 reduced at various temperatures (Fig. 6a) and Pd-TiO_2 with various Pd loadings (Fig. 6b). Samples 0.2Pd-TiO_2(150°C), 0.2Pd-TiO_2(250°C), and 0.2Pd-TiO_2 (350°C) showed the Pd $3d_{5/2}$ binding energy (BE) at 336.5, 336.3, and 336.1 eV, respectively. The BE of the Pd $3d_{5/2}$ core level for Pd foil in the literature value is 335.1 eV [52], which is lower than the present Pd $3d_{5/2}$ core level in this study, verifying the higher oxidation state of atomic dispersed Pd in nanoanatse TiO_2 compared with the Pd foil. The BE of element is closely related to its electronic structure [53]. Generally, the electron exchange and the variation of electron cloud density are reflected directly through the shift of BE. As shown in Fig. 6a, the BE of Pd $3d_{5/2}$ core levels corresponding to 0.2Pd-TiO_2 reduced slightly with the increase of reduction temperature. However, note that the shift of BE triggered by the varying reduction temperature was relatively inconspicuous. In comparison, the BE of Pd $3d_{5/2}$ in Pd-TiO_2 with various Pd loadings showed a distinctive variation: it decreased rapidly with the increase of Pd loading, which might be associated with the aggregation of Pd atoms at higher loadings.

Based on previous reports, the wavenumber of CO adsorption peak could give information on the oxidation state of the surface metal species. Especially, the different CO bonding modes on the atomically dispersed metal atoms and nanoparticles can clearly differentiate the oxidation state of metal atoms [1,54,55]. For instance, the CO stretches at 2080–2100 cm^{-1} were assigned to CO linearly adsorbed on the positively charged Pd atoms. The CO adsorption at ca. 2060, 1860 and 1950 cm^{-1} was ascribed to the CO linearly bonded on Pd nanoparticles, bridge-bonded CO on the adjacent Pd atoms and CO adsorbed on the interface between Pd atoms and the carrier, respectively.

The CO adsorption behavior on various Pd-TiO_2 catalysts was measured to identify the oxidation state of Pd atoms on nanoanatase TiO_2. As shown in Fig. 7, no CO adsorption peak was detected on 0.2Pd-TiO_2(O); however 0.2Pd-TiO_2(150°C) showed a CO adsorption band centered at around 2098 cm^{-1}, which could be ascribed to linearly adsorbed CO on single-atom Pd species. Besides, CO DRIFTS on Pd-TiO_2 prepared in the absence of P123 was also performed (Fig. S6). A broad peak at around 1850 cm^{-1} that was assigned to bridged-bonded CO on Pd nanoparticles was observed, indicating the important role of P123 in the formation of single-atom Pd species.

In the extended X-ray absorption fine structure spectra (EXAFS), the Pd–Pd contribution at ca. 2.48 Å was absent in the k2-weighted EXAFS (Fig. 8a) in 0.2Pd-TiO_2 (150°C). The only prominent shell is centered at approximately 1.85 Å arising from Pd-O contribution, indicating that Pd species exist predominantly as isolated atoms on an oxide support [56]. As shown in Fig. 8b, the white line intensity of Pd in 0.2Pd-TiO_2(150°C) was higher than that of Pd foil, again suggesting that Pd was positively charged. Those results were consistent with the CO adsorption study that the Pd atoms were atomically dispersed on nanoscale anatase TiO_2.

Catalytic tests

Selective hydrogenation of phenylacetylene to styrene is an important reaction in industry. The phenylacetylene might poison the catalysts for styrene polymerization and reduce the purity of the products. Pd is an excellent hydrogenation catalyst for the hydrogenation of both al-

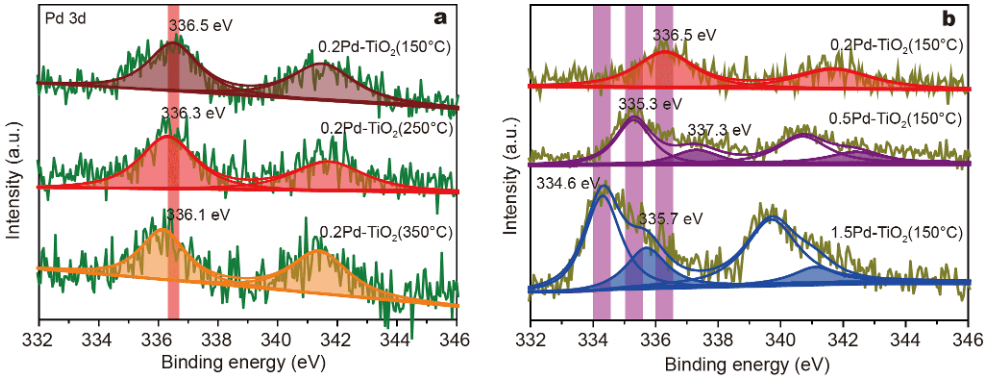

Figure 6 XPS spectra for the Pd 3d core level of 0.2Pd-TiO_2 reduced at different temperatures (a) and Pd-TiO_2 with different Pd loadings reduced at 150°C (b).

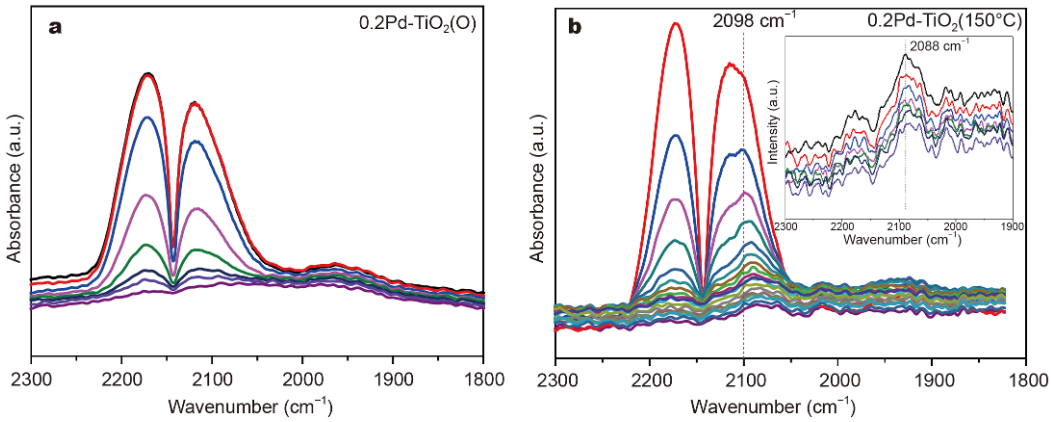

Figure 7 DRIFTS spectra of CO adsorption on (a) 0.2Pd-TiO_2(O), (b) 0.2Pd-TiO_2(150°C).

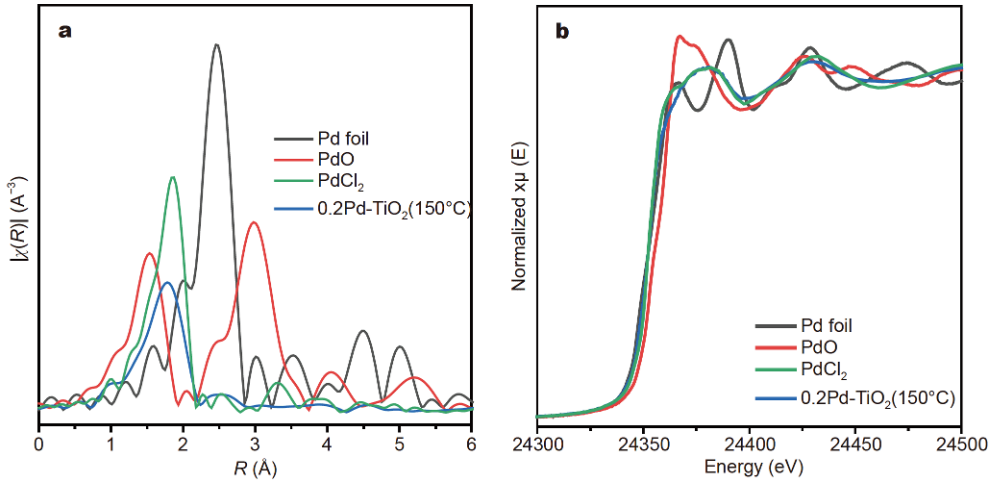

Figure 8 (a) Fourier transforms of k2-weighted Pd K-edge EXAFS experimental data for Pd foil, PdO, $PdCl_2$ and 0.2Pd-TiO_2(150°C); (b) X-ray absorption near edge structure (XANES) of Pd K-edge for Pd foil, PdO, $PdCl_2$ and 0.2Pd-TiO_2(150°C).

kynes and alkenes [57–59]. In this work, the effect of Pd loading on phenylacetylene hydrogenation activity over Pd-TiO_2 catalysts prepared by the self-assembly method was studied. As summarized in Table 2, as the H_2 pressure increased from 4 to 10 bar, the phenylacetylene conversion was enhanced for 1.5Pd-TiO_2(150°C), 0.5Pd-TiO_2(150°C) and 0.2Pd-TiO_2(150°C) catalysts. At the same H_2 pressure, the phenylacetylene conversion decreased substantially as Pd loading was increased from 0.2 to 1.5 wt% under similar reaction conditions. Both CO adsorption and EXAFS proved that single Pd atoms were dominant on 0.2Pd-TiO_2(150°C). In the blank experiment using pure TiO_2, no detectable amount of styrene or ethylbenzene was observed, confirming that TiO_2 support alone was inactive. Plausibly, Pd nanoparticles formed when the Pd loading was above 0.5%. Much smaller percentage of single Pd atoms were exposed on the surface of TiO_2 on 0.5Pd-TiO_2(150°C) and 1.5Pd-TiO_2(150°C) samples, explaining why 0.2Pd-TiO_2(150°C) showed better activity with a turnover frequency (TOF) of more than 8000 h^{-1}. In heterogeneous catalysis, the improvement of catalytic performance is usually accompanied by the decrease of selectivity towards desired products due to the existence of scaling relationship, which bridges the reaction energy with the adsorption energy of substrates/intermediates [60]. The time-dependent catalytic performance of 0.2Pd-TiO_2(150°C), 0.5Pd-TiO_2(150°C), and 1.5Pd-TiO_2(150°C) was shown in Fig. S7. 0.2Pd-TiO_2(150°C) sample with dominant single-atom Pd species showed 91% styrene selectivity at almost full phenylacetylene conversion, while 0.5Pd-TiO_2(150°C) and 1.5Pd-TiO_2(150°C) catalysts showed much lower conversion

Table 2 Catalytic performance for phenylacetylene hydrogenation over various catalysts

Entry	Catalyst	Amount (mg)	Reaction time (min)	Pressure H_2 (bar)	Conversion (%)	Selectivity (%)		Mass normalized reaction rate (mmol g^{-1}_{cat} h^{-1})	TOF (h^{-1})
						Styrene	Ethylbenzene		
1	1.5Pd-TiO_2(150°C)	3.3	30	10	56	91	9	6.92	4912
2				8	30	95	5	3.71	2631
3				6	25	95	5	3.09	2193
4				4	7	97	3	0.87	614
5			45	10	98	85	15	8.08	5730
6	0.5Pd-TiO_2(150°C)	10	30	10	67	90	10	2.73	5818
7				8	37	93	7	1.51	3212
8				6	30	93	7	1.22	2605
9				4	13	95	5	0.53	1129
10			40	10	97	88	12	2.97	6317
11	0.2Pd-TiO_2(150°C)	25	30	10	99	91	9	1.62	8596
12				8	86	92	8	1.40	7467
13				6	50	95	5	0.82	4341
14				4	16	96	4	0.26	1389
15	Pd/C(10wt%)	5	30	1	95	83	17	7.75	822
16				3	100	32	68	8.16	865
17	0.2Pd-TiO_2(post-150°C)	25	30	10	79	86	14	1.29	6772
18	TiO_2	25	30	0	0	0	0	0	0
19	Lindlar catalyst	10	60	10	99	87	13	2.02	214
20[a]	0.2Pd-TiO_2(150°C)	25	30	10	100	0	100	1.63	8682

Reaction conditions: 3 mL methanol, 224 μL phenylacetylene, room temperature. a) Styrene hydrogenation, 234 μL styrene.

with similar styrene selectivity (90%–91%), indicating that single-atom Pd exhibited superior activity and selectivity in phenylacetylene hydrogenation in comparison with nanoparticle counterparts and commercial Lindlar catalyst (selectivity 87%, Entry 19).

The catalytic performance of 0.2Pd-TiO_2(post-150°C) prepared by the post-impregnation method and the commercial Pd/C (10 wt%) was also measured. Compared with 0.2Pd-TiO_2 synthesized by the self-assembly method, 0.2Pd-TiO_2(post-150°C) exhibited poorer activity and selectivity. Although 10 wt% Pd/C showed satisfactory phenylacetylene hydrogenation activity, the selectivity towards styrene was low. It is generally believed that H_2 undergoes homolytic dissociation on Pd nanoparticles into H atoms with minimally polarized bonds ($H^{\delta-}$) [61]. In this case, Pd nanoparticles are capable of inducing the density of active hydrogen atom around the Pd particles, and alkynes would undergo the adsorption and activation process and interact with the hydrogen atom. In principle, the generated olefin could be unceasingly activated and interact with the surrounding activated hydrogen atoms to produce the final hydrogenated alkane. Compared with single Pd atoms, Pd nanoparticles provide more activated hydrogen species for the hydrogenation of alkene to alkane, thereby inducing low selectivity towards alkene.

The advantage of single-atom Pd dispersed on TiO_2 in semi-hydrogenation of phenylacetylene is tentatively proposed (Scheme 2). Specifically, single Pd atoms adsorb the H_2 molecule and dissociate it into two hydrogen atoms [62]. In the meantime, the phenylacetylene molecules adsorbed on Pd atoms as a result of the interaction between π bond of triple bonds and the unoccupied d-orbital of Pd are easily activated, followed by the cleavage of π bond. The H atoms formed around Pd atoms then attack the activated phenylacetylene to form styrene [63,64]. Styrene could also be activated and further interact with the dissociated H atoms to form ethylbenzene. We conducted a control experiment using single-atom 0.2Pd-TiO_2(150°C) catalyst for styrene hydrogenation. Styrene was fully converted to ethylbenzene under similar conditions as used in the conversion of phenylacetylene

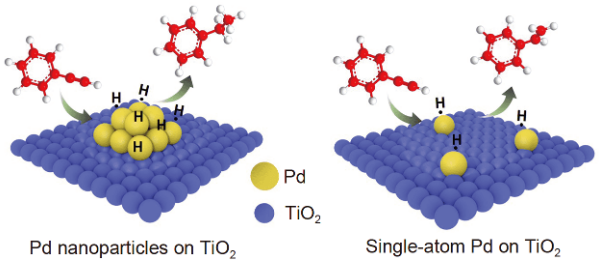

Scheme 2 Schematic illustration for the hydrogenation of phenylacetylene on Pd nanoparticles supported on TiO_2 (left) and single-atom Pd on TiO_2 (right).

(entry 20, table 3), suggesting that the catalyst is not intrinsically inert for C=C bond hydrogenation. Rather, it is not able to conduct consecutive triple and double bond hydrogenation to form alkanes, possibly due to the lack of nearby hydrogen as proposed above. Another explanation is that competitive adsorption between phenylacetylene and styrene exists on 0.2Pd-TiO_2(150°C), and the adsorption of phenylacetylene is stronger than that of styrene on atomically dispersed Pd. As a result, single Pd atoms decrease the chance of further hydrogenation due to facile desorption of styrene enabled by phenylacetylene replacement.

CONCLUSION

In summary, we developed a single-atom Pd catalyst supported on nanoscale TiO_2 with well-controlled Pd loadings. The prepared single Pd atom catalyst showed superior activity and selectivity in the selective semi-hydrogenation of phenylacetylene, compared with commercial Pd/C catalyst and Pd-TiO_2 prepared by post-impregnation method. The excellent catalytic performance could be attributed to unique electronic structure and nanoscale TiO_2. This work highlights the potential of making a series of SACs on nanosized supports for a range of reactions.

Received 17 January 2020; accepted 15 February 2020; published online 5 March 2020

1 Qiao B, Wang A, Yang X, *et al.* Single-atom catalysis of CO oxidation using Pt_1/FeO_x. Nat Chem, 2011, 3: 634–641
2 Hülsey MJ, Zhang J, Yan N. Harnessing the wisdom in colloidal chemistry to make stable single-atom catalysts. Adv Mater, 2018, 30: 1802304
3 Ding S, Hülsey MJ, Pérez-Ramírez J, *et al.* Transforming energy with single-atom catalysts. Joule, 2019, 3: 2897–2929
4 Wang A, Li J, Zhang T. Heterogeneous single-atom catalysis. Nat Rev Chem, 2018, 2: 65–81
5 Cui X, Li W, Ryabchuk P, *et al.* Bridging homogeneous and heterogeneous catalysis by heterogeneous single-metal-site catalysts. Nat Catal, 2018, 1: 385–397
6 Giannakakis G, Flytzani-Stephanopoulos M, Sykes ECH. Single-atom alloys as a reductionist approach to the rational design of heterogeneous catalysts. Acc Chem Res, 2019, 52: 237–247
7 Flytzani-Stephanopoulos M. Supported metal catalysts at the single-atom limit—a viewpoint. Chin J Catal, 2017, 38: 1432–1442
8 Liu L, Corma A. Metal catalysts for heterogeneous catalysis: from single atoms to nanoclusters and nanoparticles. Chem Rev, 2018, 118: 4981–5079
9 Yang XF, Wang A, Qiao B, *et al.* Single-atom catalysts: a new frontier in heterogeneous catalysis. Acc Chem Res, 2013, 46: 1740–1748
10 Flytzani-Stephanopoulos M. Gold atoms stabilized on various supports catalyze the water–gas shift reaction. Acc Chem Res, 2014, 47: 783–792
11 Liu J. Catalysis by supported single metal atoms. ACS Catal, 2017, 7: 34–59
12 Wang H, Lu J. Atomic layer deposition: a gas phase route to bottom-up precise synthesis of heterogeneous catalyst. Acta Phys Chim Sin, 2018, 34: 1334–1357
13 Liu JC, Tang Y, Wang YG, *et al.* Theoretical understanding of the stability of single-atom catalysts. Natl Sci Rev, 2018, 5: 638–641
14 Wang J, Li Z, Wu Y, *et al.* Fabrication of single-atom catalysts with precise structure and high metal loading. Adv Mater, 2018, 30: 1801649
15 Wang X, Li Z, Qu Y, *et al.* Review of metal catalysts for oxygen reduction reaction: from nanoscale engineering to atomic design. Chem, 2019, 5: 1486–1511
16 Chen Z, Vorobyeva E, Mitchell S, *et al.* Single-atom heterogeneous catalysts based on distinct carbon nitride scaffolds. Natl Sci Rev, 2018, 5: 642–652
17 Zhang L, Doyle-Davis K, Sun X. Pt-based electrocatalysts with high atom utilization efficiency: from nanostructures to single atoms. Energy Environ Sci, 2019, 12: 492–517
18 Chen Y, Ji S, Chen C, *et al.* Single-atom catalysts: synthetic strategies and electrochemical applications. Joule, 2018, 2: 1242–1264
19 Zhang B, Sun G, Ding S, *et al.* Atomically dispersed Pt_1–polyoxometalate catalysts: how does metal–support interaction affect stability and hydrogenation activity? J Am Chem Soc, 2019, 141: jacs.9b00486
20 Ge J, He D, Chen W, *et al.* Atomically dispersed Ru on ultrathin Pd nanoribbons. J Am Chem Soc, 2016, 138: 13850–13853
21 Lang R, Xi W, Liu JC, *et al.* Non defect-stabilized thermally stable single-atom catalyst. Nat Commun, 2019, 10: 234
22 Li X, Huang X, Xi S, *et al.* Single cobalt atoms anchored on porous N-doped graphene with dual reaction sites for efficient fenton-like catalysis. J Am Chem Soc, 2018, 140: 12469–12475
23 Li X, Yang X, Huang Y, *et al.* Supported noble-metal single atoms for heterogeneous catalysis. Adv Mater, 2019, 31: 1902031
24 Shao X, Yang X, Xu J, *et al.* Iridium single-atom catalyst performing a quasi-homogeneous hydrogenation transformation of CO_2 to formate. Chem, 2019, 5: 693–705
25 Su X, Yang XF, Huang Y, *et al.* Single-atom catalysis toward efficient CO_2 conversion to CO and formate products. Acc Chem Res, 2019, 52: 656–664
26 Zheng N, Zhang T. Preface: single-atom catalysts as a new generation of heterogeneous catalysts. Natl Sci Rev, 2018, 5: 625
27 Zhang B, Asakura H, Zhang J, *et al.* Stabilizing a platinum$_1$ single-atom catalyst on supported phosphomolybdic acid without compromising hydrogenation activity. Angew Chem Int Ed, 2016, 55:

8319–8323
28 Qin R, Liu P, Fu G, *et al.* Strategies for stabilizing atomically dispersed metal catalysts. Small Methods, 2018, 2: 1700286
29 Grosso-Giordano NA, Hoffman AS, Boubnov A, *et al.* Dynamic reorganization and confinement of Ti^{IV} active sites controls olefin epoxidation catalysis on two-dimensional zeotypes. J Am Chem Soc, 2019, 141: 7090–7106
30 Jones J, Xiong H, DeLaRiva AT, *et al.* Thermally stable single-atom platinum-on-ceria catalysts *via* atom trapping. Science, 2016, 353: 150–154
31 Liu P, Zhao Y, Qin R, *et al.* Photochemical route for synthesizing atomically dispersed palladium catalysts. Science, 2016, 352: 797–800
32 Nie L, Mei D, Xiong H, *et al.* Activation of surface lattice oxygen in single-atom Pt/CeO_2 for low-temperature CO oxidation. Science, 2017, 358: 1419–1423
33 Chen C, Wu D, Li Z, *et al.* Ruthenium-based single-atom alloy with high electrocatalytic activity for hydrogen evolution. Adv Energy Mater, 2019, 9: 1803913
34 Chen Z, Gong W, Liu Z, *et al.* Coordination-controlled single-atom tungsten as a non-3d-metal oxygen reduction reaction electrocatalyst with ultrahigh mass activity. Nano Energy, 2019, 60: 394–403
35 Li Y, Hao J, Song H, *et al.* Selective light absorber-assisted single nickel atom catalysts for ambient sunlight-driven CO_2 methanation. Nat Commun, 2019, 10: 2359
36 Chen W, Pei J, He CT, *et al.* Rational design of single molybdenum atoms anchored on N-doped carbon for effective hydrogen evolution reaction. Angew Chem Int Ed, 2017, 56: 16086–16090
37 Han L, Liu X, Chen J, *et al.* Atomically dispersed molybdenum catalysts for efficient ambient nitrogen fixation. Angew Chem Int Ed, 2019, 58: 2321–2325
38 Yang F, Song P, Liu X, *et al.* Highly efficient CO_2 electroreduction on ZnN_4-based single-atom catalyst. Angew Chem Int Ed, 2018, 57: 12303–12307
39 Yan J, Kong L, Ji Y, *et al.* Single atom tungsten doped ultrathin α-$Ni(OH)_2$ for enhanced electrocatalytic water oxidation. Nat Commun, 2019, 10: 2149
40 Zhu Y, Sun W, Luo J, *et al.* A cocoon silk chemistry strategy to ultrathin N-doped carbon nanosheet with metal single-site catalysts. Nat Commun, 2018, 9: 3861
41 Shan J, Li M, Allard LF, *et al.* Mild oxidation of methane to methanol or acetic acid on supported isolated rhodium catalysts. Nature, 2017, 551: 605–608
42 Zhang Z, Zhu Y, Asakura H, *et al.* Thermally stable single atom Pt/m-Al_2O_3 for selective hydrogenation and co oxidation. Nat Commun, 2017, 8: 16100
43 Vilé G, Albani D, Nachtegaal M, *et al.* A stable single-site palladium catalyst for hydrogenations. Angew Chem Int Ed, 2015, 54: 11265–11269
44 Yan H, Cheng H, Yi H, *et al.* Single-atom Pd_1/graphene catalyst achieved by atomic layer deposition: remarkable performance in selective hydrogenation of 1,3-butadiene. J Am Chem Soc, 2015, 137: 10484–10487
45 Pei GX, Liu XY, Yang X, *et al.* Performance of Cu-alloyed Pd single-atom catalyst for semihydrogenation of acetylene under simulated front-end conditions. ACS Catal, 2017, 7: 1491–1500
46 Kyriakou G, Boucher MB, Jewell AD, *et al.* Isolated metal atom geometries as a strategy for selective heterogeneous hydrogenations. Science, 2012, 335: 1209–1212
47 Lin R, Albani D, Fako E, *et al.* Design of single gold atoms on nitrogen-doped carbon for molecular recognition in alkyne semihydrogenation. Angew Chem Int Ed, 2019, 58: 504–509
48 Huang F, Deng Y, Chen Y, *et al.* Anchoring Cu_1 species over nanodiamond-graphene for semi-hydrogenation of acetylene. Nat Commun, 2019, 10: 4431
49 Wang J, Zhao D, Yang P, *et al.* Confined space synthesis of mesoporous silica nanoparticles with a three dimensionally ordered close-packing structure. Mater Des, 2016, 98: 41–46
50 Jiao Y, Chen X, He F, *et al.* Simple preparation of uniformly distributed mesoporous Cr/TiO_2 microspheres for low-temperature catalytic combustion of chlorobenzene. Chem Eng J, 2019, 372: 107–117
51 Liu Y, Zhou S, Yang F, *et al.* Degradation of phenol in industrial wastewater over the $F–Fe/TiO_2$ photocatalysts under visible light illumination. Chin J Chem Eng, 2016, 24: 1712–1718
52 Rameshan C, Weilach C, Stadlmayr W, *et al.* Steam reforming of methanol on PdZn near-surface alloys on Pd(111) and Pd foil studied by *in-situ* XPS, LEIS and PM-IRAS. J Catal, 2010, 276: 101–113
53 Yang F, Tang J, Ou R, *et al.* Fully catalytic upgrading synthesis of 5-ethoxymethylfurfural from biomass-derived 5-hydroxymethylfurfural over recyclable layered-niobium-molybdate solid acid. Appl Catal B-Environ, 2019, 256: 117786
54 Gu XK, Qiao B, Huang CQ, *et al.* Supported single Pt_1/Au_1 atoms for methanol steam reforming. ACS Catal, 2014, 4: 3886–3890
55 Qiao B, Liu J, Wang YG, *et al.* Highly efficient catalysis of preferential oxidation of CO in H_2-rich stream by gold single-atom catalysts. ACS Catal, 2015, 5: 6249–6254
56 Zhou S, Shang L, Zhao Y, *et al.* Pd single-atom catalysts on nitrogen-doped graphene for the highly selective photothermal hydrogenation of acetylene to ethylene. Adv Mater, 2019, 31: 1900509
57 Karakhanov EA, Maximov AL, Zolotukhina AV. Selective semihydrogenation of phenyl acetylene by Pd nanocatalysts encapsulated into dendrimer networks. Mol Catal, 2019, 469: 98–110
58 Li X, Pan Y, Yi H, *et al.* Mott–schottky effect leads to alkyne semihydrogenation over Pd-nanocube@N-doped carbon. ACS Catal, 2019, 9: 4632–4641
59 Liu Y, Wang Q, Wu L, *et al.* Tunable bimetallic $Au–Pd@CeO_2$ for semihydrogenation of phenylacetylene by ammonia borane. Nanoscale, 2019, 11: 12932–12937
60 Sun G, Zhao ZJ, Mu R, *et al.* Breaking the scaling relationship *via* thermally stable Pt/Cu single atom alloys for catalytic dehydrogenation. Nat Commun, 2018, 9: 4454
61 Syrenova S, Wadell C, Nugroho FAA, *et al.* Hydride formation thermodynamics and hysteresis in individual Pd nanocrystals with different size and shape. Nat Mater, 2015, 14: 1236–1244
62 Navalikhina MD, Kavalerskaya NE, Lokteva ES, *et al.* Selective hydrogenation of phenylacetylene on Ni and Ni-Pd catalysts modified with heteropoly compounds of the keggin type. Russ J Phys Chem, 2012, 86: 1800–1807
63 Markov PV, Mashkovsky IS, Bragina GO, *et al.* Particle size effect in liquid-phase hydrogenation of phenylacetylene over Pd catalysts: experimental data and theoretical analysis. Chem Eng J, 2019, 358: 520–530
64 Yang L, Yu S, Peng C, *et al.* Semihydrogenation of phenylacetylene over nonprecious Ni-based catalysts supported on AlSBA-15. J Catal, 2019, 370: 310–320

Acknowledgements This work was supported by the National University of Singapore Flagship Green Energy Program (#R-279-000-553-646 and R-279-000-553-731), the National Natural Science Foundation of China (21908085), and the Natural Science Foundation of Jiangsu Province, China (BK20190961). We also thank Prof. Hiroyuki Asakura from Kyoto University for conducting X-ray absorption spectroscopy measurements.

Author contributions Song H started the project and prepared the catalysts. Yang F carried out the catalyst synthesis, characterization and catalytic performance test. Yang F wrote the manuscript. Yan N and Ding S supervised the project and revised the manuscript. All authors contributed to the general discussion.

Conflict of interest The authors declare no conflict of interest.

Supplementary information Supporting data are available in the online version of the paper.

Fu Yang received his PhD degree from Nanjing Tech University under the supervision of Prof. Yan Kong. During the PhD pursuing period, he worked with Prof. Ning Yan at the National University of Singapore as a China Scholarship Council (CSC) exchange student. After finishing his PhD, he joined Jiangsu University of Science and Technology as a lecturer. His research focuses on the development functional molecular sieve catalyst and nanostructural functional composite materials specific to heterogeneous selective catalytic oxidation/hydrogenation reaction and volatile organic compounds (VOCs) treatment.

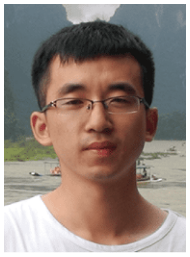

Shipeng Ding received his BSc (2012) and MSc (2015) degrees in environmental engineering from Lanzhou University and Chinese Academy of Sciences, respectively. Since 2016, he has been pursuing his PhD in chemical engineering under the supervision of Prof. Ning Yan at the National University of Singapore, focusing on the synthesis, characterization and utilization of single-atom catalysts.

Ning Yan received BSc and PhD degrees in chemistry from Peking University working with Prof. Yuan Kou. After a Marie Curie Fellowship at the École Polytechnique Fédérale de Lausanne in Switzerland with Prof. Paul Dyson, he joined the Department of Chemical and Biomolecular Engineering at the National University of Singapore as an assistant professor in 2012 and was promoted to a tenured associate professor in 2018. Ning Yan works actively in advanced catalysis, renewable energy, and sustainable chemistry, for which he was duly recognized by recent awards from the Royal Society of Chemistry, American Chemical Society and National University of Singapore, among others.

纳米氧化钛负载的单原子钯催化剂用于苯乙炔选择性加氢

杨福[1,2], 丁世鹏[1*], 宋红兵[3], 颜宁[1*]

摘要 单原子催化剂(SACs)兼具均相和非均相催化剂的优点, 具有独特的电子结构, 在某些反应中呈现出优异的催化性能. 本文采用自组装方法将单原子Pd分散于纳米级的TiO_2载体上, 采用N_2吸附/解吸、XRD、TEM、XPS、DRIFT和XAS对催化剂的结构进行了表征. 在苯乙炔选择加氢制苯乙烯中, 催化剂表现出优异的活性和选择性. 在室温条件下, 单原子催化剂0.2 wt% Pd-TiO_2(150°C)的TOF达8000 h^{-1}以上, 苯乙烯选择性维持在90%以上. 当Pd负载量增加到0.5 wt%和1.5 wt%时, Pd物种聚集形成纳米颗粒, 从而使活性下降. 该方法制备的单原子0.2Pd-TiO_2催化剂催化性能显著高于商品化10%Pd/C以及浸渍法制备的0.2Pd/TiO_2催化剂.

